Crystal structure of alectinib hydrochloride Type I, $C_{30}H_{35}N_4O_2Cl$

James A. Kaduk,[1,2,a] Megan M. Rost,[3] Anja Dosen,[3] and Thomas N. Blanton[3]
[1]*Illinois Institute of Technology, 3101 S. Dearborn St., Chicago, IL 60616, USA*
[2]*North Central College, 131 S. Loomis St., Naperville, IL 60540, USA*
[3]*ICDD, 12 Campus Blvd., Newtown Square, PA 19073-3273, USA*

(Received 30 January 2024; accepted 26 March 2024)

The crystal structure of alectinib hydrochloride has been solved and refined using synchrotron X-ray powder diffraction data and optimized using density functional theory techniques. Alectinib hydrochloride crystallizes in space group $P2_1/n$ (#14) with the following parameters: $a = 12.67477(7)$, $b = 10.44076(5)$, $c = 20.38501(12)$ Å, $\beta = 93.1438(7)°$, $V = 2693.574(18)$ Å^3, and $Z = 4$ at 295 K. The crystal structure consists of stacks of molecules along the *b*-axis, and the stacks contain chains of strong N–H···Cl hydrogen bonds. One density functional theory calculation moved a proton from an N atom to the Cl, but another calculation yielded a more chemically reasonable result. The powder pattern has been submitted to ICDD for inclusion in the Powder Diffraction File™ (PDF®)

[doi:10.1017/S0885715624000204]

Key words: alectinib, Alcensa®, crystal structure, Rietveld refinement, density functional theory

In memory of Earle R. Ryba of The Pennsylvania State University

I. INTRODUCTION

Alectinib hydrochloride (marketed under the trade name Alcensa®) is used to treat non-small-cell-lung cancer that has spread to other parts of the body (metastasis). The systematic name of alectinib hydrochloride (CAS Registry Number 1256589-74-8) is 9-ethyl-6,6-dimethyl-8-(4-morpholin-4-ylpiperidin-1-yl)-11-oxo-5H-benzo[b]carbazole-3-carbonitrile hydrochloride. A two-dimensional molecular diagram of alectinib hydrochloride is shown in Figure 1.

X-ray powder diffraction data are reported for crystalline Type I of alectinib hydrochloride in European Patent EP3135671 B1 (Tanaka and Ueto, 2019; Chugai Seiyaku Kabushiki Kaisha), and Type II and Type III are claimed (Figure 2). The crystal structures have not yet been reported. A process for preparing alectinib hydrochloride and Types IV, V, and VI are claimed in International Patent Application WO2019/008520 A1 (Tomar et al., 2019; Fresenius Kabi Oncology Ltd.) and its US equivalent US 2020/0140427 A1 (Tomar et al., 2020). These Fresenius applications also claim a process for preparing alectinib free base and crystalline Form B of alectinib.

This work was carried out as part of a project (Kaduk et al., 2014) to determine the crystal structures of large-volume commercial pharmaceuticals and include high-quality powder diffraction data for them in the Powder Diffraction File (Gates-Rector and Blanton, 2019).

II. EXPERIMENTAL

Alectinib hydrochloride used in this study was a commercial reagent, purchased from TargetMol (Batch #142717), and was used as-received. The white powder was packed into a 1.5 mm diameter Kapton capillary and rotated during the measurement at ~50 Hz. The powder pattern was measured at 295 K at beamline 11-BM (Antao et al., 2008; Lee et al., 2008; Wang et al., 2008) of the Advanced Photon Source at Argonne National Laboratory using a wavelength of 0.459744(2) Å from 0.5 to 40° 2θ with a step size of 0.001° and a counting time of 0.1 s/step. The high-resolution powder diffraction data were collected using 12 silicon crystal analyzers that allow for high angular resolution, high precision, and accurate peak positions. A mixture of silicon (NIST SRM 640c) and alumina (NIST SRM 676a) standards (ratio Al_2O_3:Si = 2:1 by weight) was used to calibrate the instrument and refine the monochromatic wavelength used in the experiment.

The pattern was indexed using JADE Pro (MDI, 2023) on a primitive monoclinic unit cell with the following parameters: $a = 12.66430$, $b = 10.43968$, $c = 20.37822$ Å, $\beta = 93.21°$, $V = 2690.00$ Å^3, and $Z = 4$. The space group suggested by EXPO2014 (Altomare et al., 2013) was $P2_1/n$, which was confirmed by the successful solution and refinement of the structure. A reduced cell search of the Cambridge Structural Database (Groom et al., 2016) yielded 14 hits, but none were structures of alectinib derivatives.

The alectinib molecule was downloaded from PubChem (Kim et al., 2023) as Conformer3D_CID_49806720.sdf and

[a]Author to whom correspondence should be addressed. Electronic mail: kaduk@polycrystallography.com

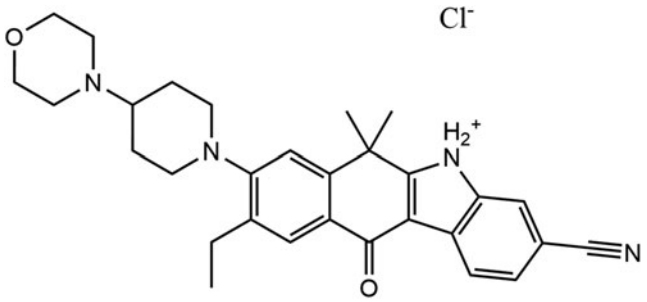

Figure 1. The two-dimensional structure of alectinib hydrochloride.

was converted into a .mol2 file using Mercury (Macrae et al., 2020). The structure was solved by Monte Carlo-simulated annealing techniques as implemented in EXPO2014 (Altomare et al., 2013) using an alectinib molecule and a Cl atom as fragments. Analysis of potential hydrogen bond interactions made it clear that N5 was protonated, and H72 was added to that atom using Materials Studio (Dassault, 2022).

Rietveld refinement was carried out with GSAS-II (Toby and Von Dreele, 2013). Only the 2.0–25.0° 2θ portion of the pattern was included in the refinements (d_{min} = 1.062 Å). All non-H-bond distances and angles were subjected to restraints based on a Mercury/Mogul Geometry Check (Bruno et al., 2004; Sykes et al., 2011). The Mogul average and standard deviation for each quantity were used as the restraint parameters. The benzene and fused 5/6 rings were restrained to be planar. The restraints contributed 5.8% to the final χ^2. The hydrogen atoms were included in calculated positions, which were recalculated during the refinement using Materials Studio (Dassault, 2022). The U_{iso} of the C, N, and O atoms were grouped by chemical similarity. The Cl atom was refined anisotropically. The U_{iso} values for the H atoms were fixed at 1.3× the U_{iso} values of the heavy atoms to which they are attached. The peak profiles were described using the generalized microstrain model (Stephens, 1999). The background was modeled using a 6-term shifted Chebyshev polynomial, with a peak at 5.87° 2θ to describe the scattering from the Kapton capillary and an amorphous component.

The final refinement of 145 variables using 23,037 observations and 105 restraints yielded the residuals R_{wp} = 0.08848 and goodness of fit = 1.16. The largest peak (0.23 Å from C25) and hole (1.63 Å from O2) in the difference Fourier map were 0.20(5) and –0.23(5) eÅ^{-3}, respectively. The final Rietveld plot is shown in Figure 3. The largest features in the normalized error plot are very small and represent subtle errors in peak shapes.

A default geometry optimization of the alectinib hydrochloride crystal structure using Vienna Ab Initio Structure Package (VASP) (Kresse and Furthmüller, 1996) through the MedeA graphical interface (Materials Design, 2016) moved H72 from N5 to Cl71. Higher-level calculations using more k-points and/or a higher energy cutoff yielded the same chemically unreasonable result. A geometry optimization (fixed experimental cell) and population analysis were carried out using CRYSTAL23 (Erba et al., 2023). The 6-31d1G basis sets for the H, C, N, and O atoms in the calculation were those of Gatti et al. (1994), and the triple-zeta basis set for Cl was that of Peintinger et al. (2013). The calculations were run on a 3.5 GHz PC using 8 k-points and the B3LYP functional and took ∼14.5 days.

III. RESULTS AND DISCUSSION

The powder pattern of the alectinib hydrochloride measured here agrees well enough with that reported for Type I (Tanaka and Ueto, 2019; Chugai Seiyaku Kabushiki Kaisha) to conclude that they represent the same material (Figure 4). The asymmetric unit contains one alectinib cation and one chloride anion (Figure 5).

The root-mean-square Cartesian displacement of the non-H atoms in the Rietveld-refined and CRYSTAL23-optimized cation structures is 0.181 Å (Figure 6); the maximum deviation is 0.419 Å at N5. The orientations of the

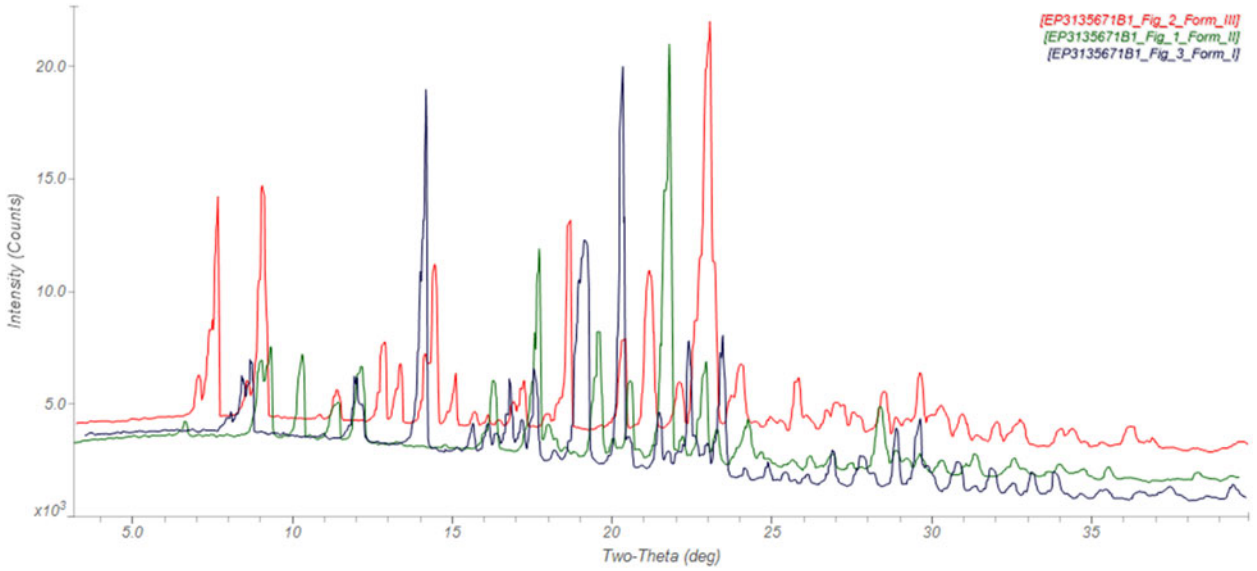

Figure 2. X-ray powder diffraction patterns of crystalline Type I (black), II (green), and III (red) of alectinib hydrochloride from European Patent EP3135671 B1 (Tanaka and Ueto, 2019; Chugai Seiyaku Kabushiki Kaisha). The patent patterns (measured using Cu K_α radiation) were digitized using UN-SCAN-IT (Silk Scientific, 2013). The image is generated using JADE Pro (MDI, 2023).

https://doi.org/10.1017/S0885715624000204 Published online by Cambridge University Press

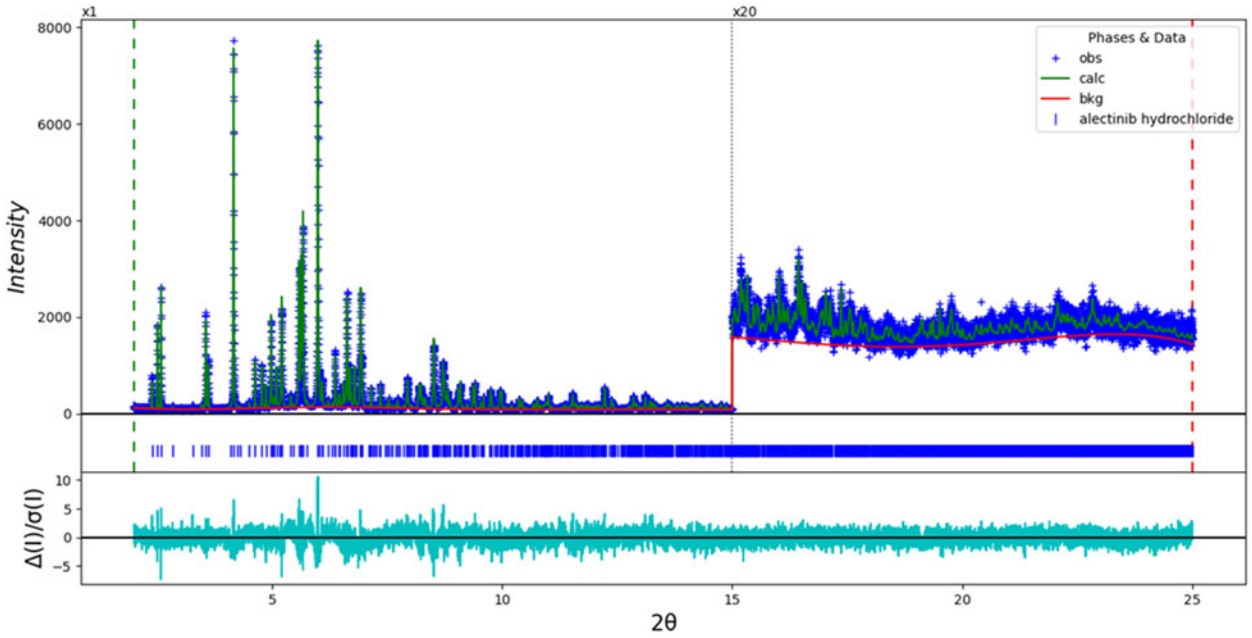

Figure 3. The Rietveld plot for the refinement of alectinib hydrochloride. The blue crosses represent the observed data points, and the green line is the calculated pattern. The cyan curve is the normalized error plot, and the red line is the background curve. The vertical scale has been multiplied by a factor of 20× for $2\theta > 15.0°$.

methyl groups differ in the refined and optimized structures, but the final H positions in the refined structure were determined by a force field; the difference with the full density functional theory (DFT) optimization is not significant. The absolute position difference between the Cl71 in the refined and optimized structures is 0.704 Å. The agreement of the cations is within the normal range for correct structures (van de Streek and Neumann, 2014) and confirms that the structure is correct. The agreement of the anion position is outside the typical range for correct organic structures but is not uncommon for inorganic anions. The chemically unreasonable VASP optimization provides a good reminder that DFT calculations are not always correct. The reminder of this discussion will emphasize the CRYSTAL23-optimized structure.

Almost all of the bond distances and bond angles fall within the normal ranges indicated by a Mercury Mogul Geometry check (Macrae et al., 2020). The C15–N5 distance of 1.476 Å (average = 1.352(16) Å, *Z*-score = 4.7) is flagged as unusual. The C35–C32–C30 angle of 116.2° (average = 119.5(5)°, *Z*-score = 6.2) is also flagged as unusual. The high *Z*-score results from the exceptionally low standard

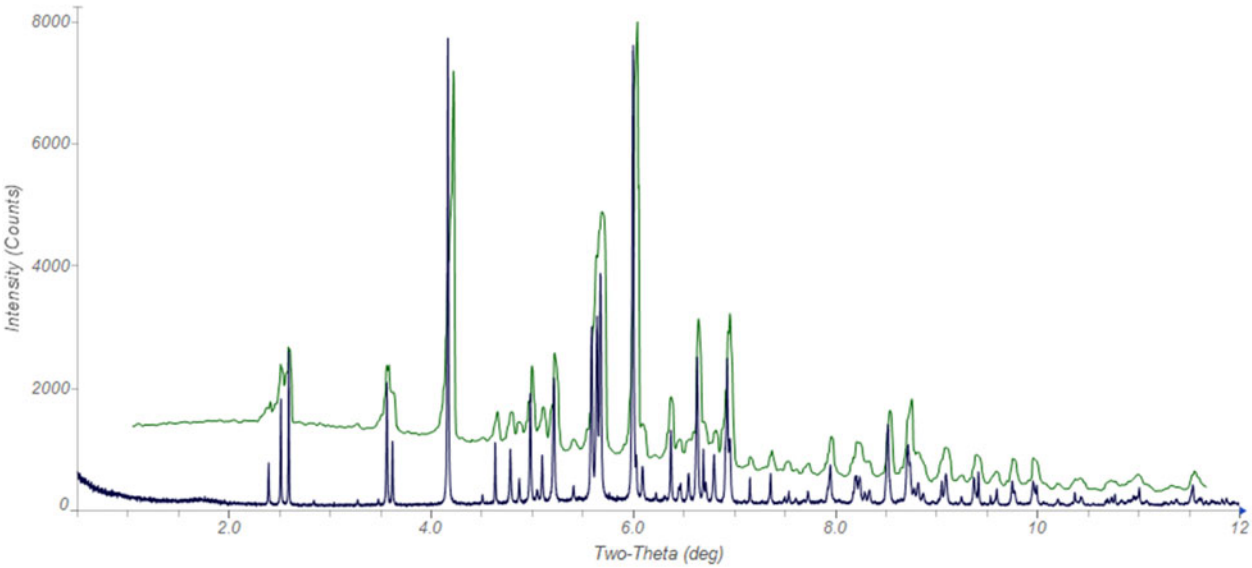

Figure 4. Comparison of the synchrotron pattern of alectinib hydrochloride from this study (black) to that of Form I from European Patent EP3135671 B1 (Tanaka and Ueto, 2019; Chugai Seiyaku Kabushiki Kaisha, green). The patent pattern (measured using Cu K_α radiation) was digitized using UN-SCAN-IT (Silk Scientific, 2013) and converted to the synchrotron wavelength of 0.459744 Å using JADE Pro (MDI, 2023). The image is generated using JADE Pro (MDI, 2023).

https://doi.org/10.1017/S0885715624000204 Published online by Cambridge University Press

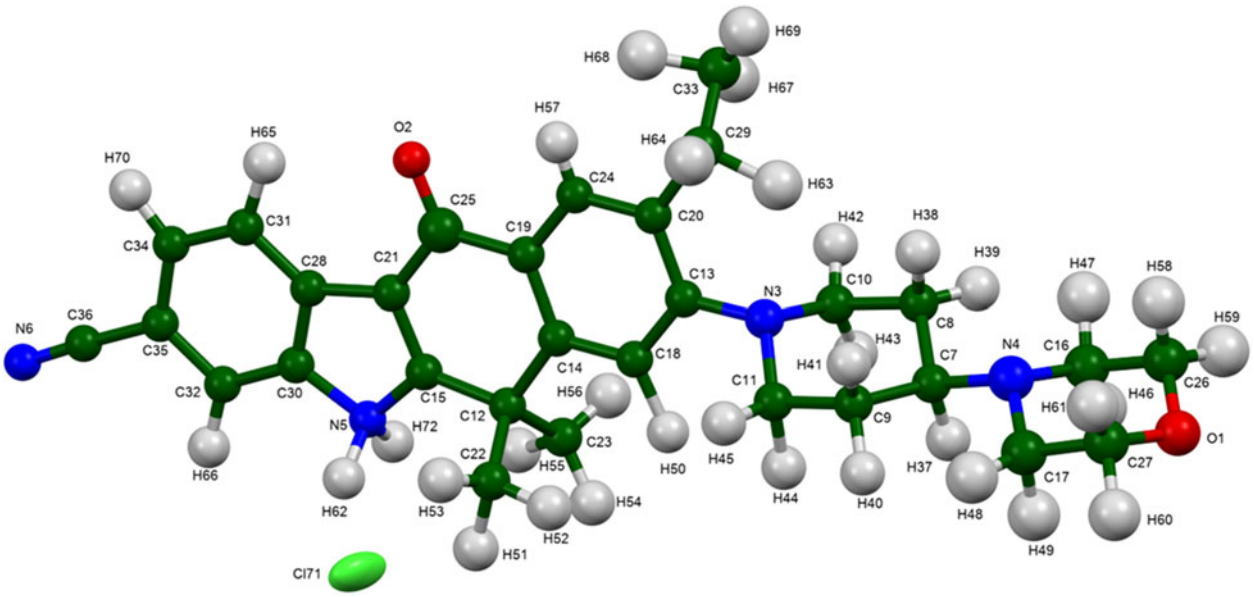

Figure 5. The asymmetric unit of alectinib hydrochloride is depicted, with the atom numbering included. The atoms are represented by 50% probability spheroids/ellipsoids. The image is generated using Mercury (Macrae et al., 2020).

uncertainty on the average. No hits were found for the C12–C15–N5 and C21–C15–N5 angles.

Quantum chemical geometry optimization of the isolated cation (DFT/B3LYP/6-31G*/water) using Spartan '20 (Wavefunction, 2022) indicated that the solid-state conformation of the cation is 6.5 kcal/mol higher in energy than the local minimum, which has a very similar conformation. The global minimum-energy conformation is 0.7 kcal/mol lower in energy and has slightly different orientations of the morpholine and piperidine rings. Intermolecular interactions thus help determine the solid-state conformation.

The crystal structure (Figure 7) consists of stacks of molecules along the *b*-axis. The mean plane of the fused ring system is approximately −2,11,12. The Mercury Aromatics Analyser indicates one moderate interaction between the fused ring systems, at 5.25 Å, and three weak interactions.

Analysis of the contributions to the total crystal energy of the structure using the Forcite module of Materials Studio (Dassault Systèmes, 2022) suggests that the intramolecular energy is dominated by angle distortion terms, as expected for a molecule containing a fused ring system. The intermolecular energy is dominated by electrostatic attractions, which, in this force field analysis, include hydrogen bonds. The hydrogen bonds are better analyzed using the results of the DFT calculation.

The protonated N5 makes two strong discrete N–H···Cl hydrogen bonds to the chloride anion (Table I). These link the cations and anions into chains along the *b*-axis. Several C–H···Cl hydrogen bonds also link the cations and anions. Intra- and inter-molecular C–H···N and C–H···O hydrogen bonds also contribute to the lattice energy.

The volume enclosed by the Hirshfeld surface of alectinib hydrochloride (Figure 8, Hirshfeld, 1977; Spackman et al., 2021) is 663.77 $Å^3$, which is 98.57% of the unit cell volume. The packing density is thus fairly typical. The only significant close contacts (red in Figure 8) involve the hydrogen bonds. The volume/non-hydrogen atom is typical at 18.2 $Å^3$.

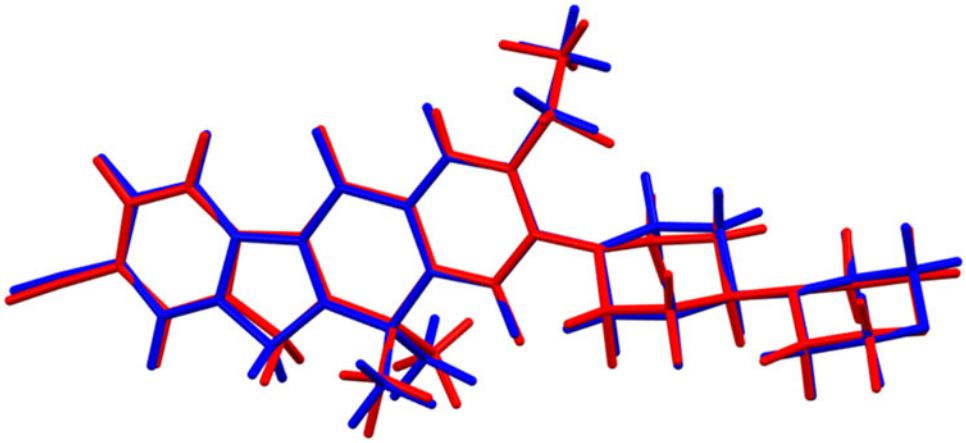

Figure 6. Comparison of the Rietveld-refined (red) and CRYSTAL23-optimized (blue) structures of alectinib hydrochloride. The rms Cartesian displacement for the cation is 0.181 Å. The image is generated using Mercury (Macrae et al., 2020).

https://doi.org/10.1017/S0885715624000204 Published online by Cambridge University Press

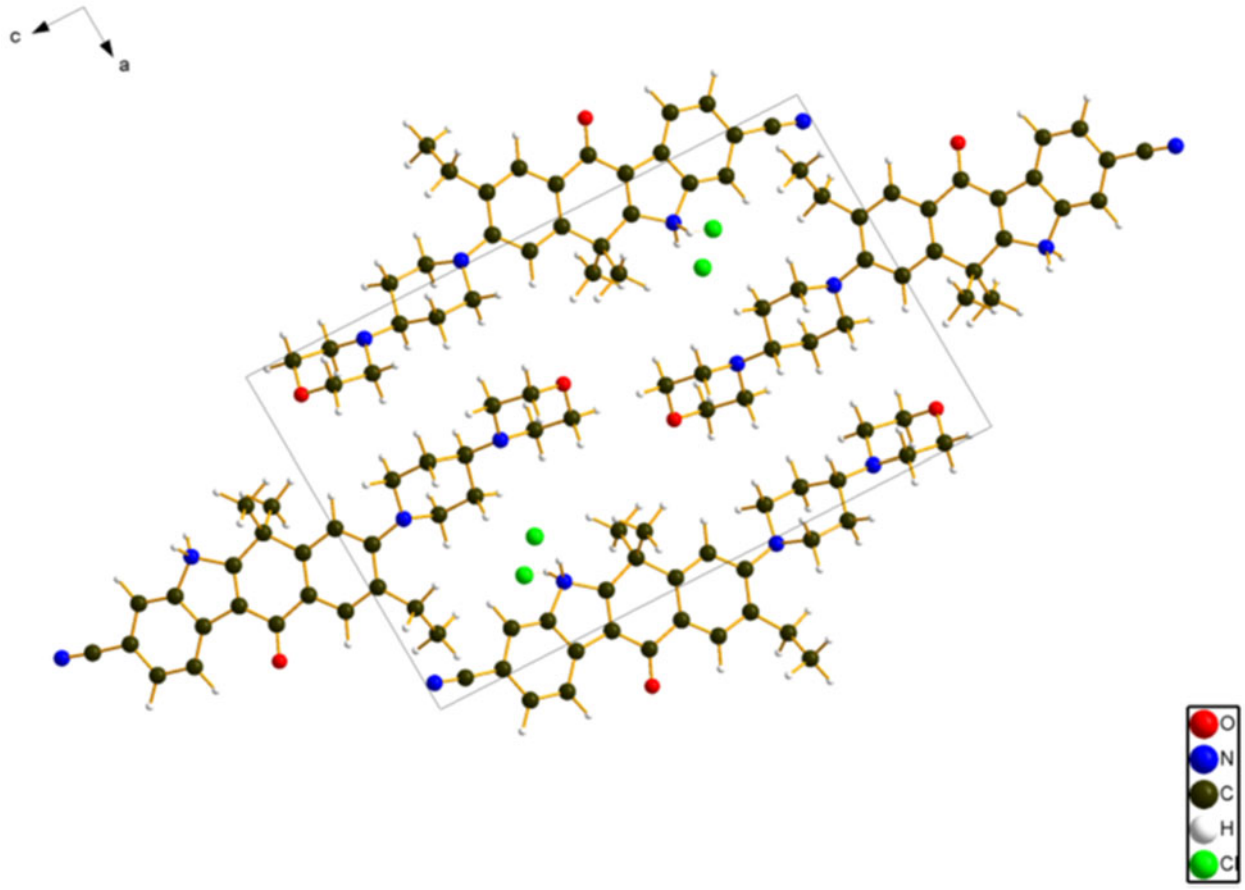

Figure 7. The crystal structure of alectinib hydrochloride is viewed down the *b*-axis. The image is generated using Diamond (Crystal Impact, 2023).

TABLE I. Hydrogen bonds (CRYSTAL23) in alectinib hydrochloride.

H-bond	D–H, Å	H···A, Å	D···A, Å	D–H···A,◦	Overlap, *e*
N5–H72···Cl71	1.068	3.037	3.044	158.3	0.108
N5–H62···Cl71	1.077	2.027	3.049	157.3	0.111
C33–H67···Cl71	1.091	2.648	3.649	152.2	0.021
C8–H38···Cl71	1.096	2.910	4.001	153.5	0.017
C10–H42···Cl71	1.090	2.872	3.683	131.2	0.016
C32–H66···Cl71	1.079	2.910	3.443	110.7	0.013
C29–H63···N3	1.091	2.499[a]	2.968	104.6	0.013
C31–H65···O2	1.081	2.612[a]	3.173	111.6	0.012
C24–H57···O2	1.085	2.440[a]	2.815	98.6	0.010
C17–H49···O2	1.103	2.400	3.368	145.6	0.010

[a]Intramolecular.

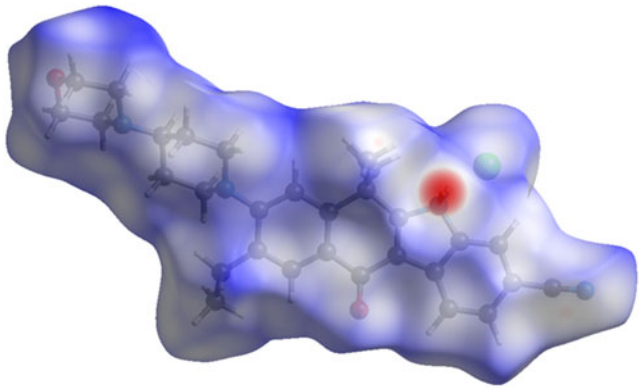

Figure 8. The Hirshfeld surface of alectinib hydrochloride. Intermolecular contacts longer than the sums of the van der Waals radii are colored blue, and contacts shorter than the sums of the radii are colored red. Contacts equal to the sums of radii are white. The image is generated using CrystalExplorer (Spackman et al., 2021).

The Bravais–Friedel–Donnay–Harker (Bravais, 1866; Friedel, 1907; Donnay and Harker, 1937) morphology suggests that we might expect roughly isotropic morphology for alectinib hydrochloride. A second-order spherical harmonic model was included in the refinement. The texture index was 1.009(0), indicating that the preferred orientation was not significant in this rotated capillary specimen.

IV. DEPOSITED DATA

The powder pattern of alectinib hydrochloride from this synchrotron data set has been submitted to ICDD for inclusion in the Powder Diffraction File. The Crystallographic Information Framework (CIF) files containing the results of the Rietveld refinement (including the raw data) and the DFT geometry optimization were deposited with the ICDD. The data can be requested at pdj@icdd.com.

ACKNOWLEDGEMENTS

Use of the Advanced Photon Source at the Argonne National Laboratory was supported by the U. S. Department of Energy, Office of Science, Office of Basic Energy Sciences under Contract No. DE-AC02-06CH11357. This

https://doi.org/10.1017/S0885715624000204 Published online by Cambridge University Press

work was partially supported by the International Centre for Diffraction Data. We thank Saul Lapidus for his assistance in the data collection.

CONFLICTS OF INTEREST

The authors have no conflicts of interest to declare.

REFERENCES

Altomare, A., C. Cuocci, C. Giacovazzo, A. Moliterni, R. Rizzi, N. Corriero, and A. Falcicchio. 2013. "EXPO2013: A Kit of Tools for Phasing Crystal Structures from Powder Data." *Journal of Applied Crystallography* 46: 1231–5.

Antao, S. M., I. Hassan, J. Wang, P. L. Lee, and B. H. Toby. 2008. "State-of-the-Art High-Resolution Powder X-ray Diffraction (HRPXRD) Illustrated with Rietveld Refinement of Quartz, Sodalite, Tremolite, and Meionite." *Canadian Mineralogist* 46: 1501–9.

Bravais, A. 1866. *Etudes Cristallographiques*. Paris, Gauthier Villars.

Bruno, I. J., J. C. Cole, M. Kessler, J. Luo, W. D. S. Motherwell, L. H. Purkis, B. R. Smith, R. Taylor, R. I. Cooper, S. E. Harris, and A. G. Orpen. 2004. "Retrieval of Crystallographically-Derived Molecular Geometry Information." *Journal of Chemical Information and Computer Sciences* 44: 2133–44.

Crystal Impact. 2023. Diamond. V. 5.0.0. Crystal Impact – Dr. H. Putz & Dr. K. Brandenburg.

Dassault Systèmes. 2022. *Materials Studio 2023*. San Diego, CA, BIOVIA.

Donnay, J. D. H., and D. Harker. 1937. "A New Law of Crystal Morphology Extending the Law of Bravais." *American Mineralogist* 22: 446–47.

Erba, A., J. K. Desmarais, S. Casassa, B. Civalleri, L. Donà, I. J. Bush, B. Searle, L. Maschio, L.-E. Daga, A. Cossard, C. Ribaldone, E. Ascrizzi, N. L. Marana, J.-P. Flament, and B. Kirtman. 2023. "CRYSTAL23: A Program for Computational Solid State Physics and Chemistry." *Journal of Chemical Theory and Computation* 19: 6891–932. doi:10.1021/acs.jctc.2c00958.

Friedel, G. 1907. "Etudes sur la loi de Bravais." *Bulletin de la Société Française de Minéralogie* 30: 326–455.

Gates-Rector, S., and T. N. Blanton. 2019. "The Powder Diffraction File: A Quality Materials Characterization Database." *Powder Diffraction* 39: 352–60.

Gatti, C., V. R. Saunders, and C. Roetti. 1994. "Crystal-Field Effects on the Topological Properties of the Electron-Density in Molecular Crystals – the Case of Urea." *Journal of Chemical Physics* 101: 10686–96.

Groom, C. R., I. J. Bruno, M. P. Lightfoot, and S. C. Ward. 2016. "The Cambridge Structural Database." *Acta Crystallographica Section B: Structural Science, Crystal Engineering and Materials* 72: 171–9.

Hirshfeld, F. L. 1977. "Bonded-Atom Fragments for Describing Molecular Charge Densities." *Theoretica Chemica Acta* 44: 129–38.

Kaduk, J. A., C. E. Crowder, K. Zhong, T. G. Fawcett, and M. R. Suchomel. 2014. "Crystal Structure of Atomoxetine Hydrochloride (Strattera), $C_{17}H_{22}NOCl$." *Powder Diffraction* 29: 269–73.

Kim, S., J. Chen, T. Cheng, A. Gindulyte, J. He, S. He, Q. Li, B. A. Shoemaker, P. A. Thiessen, B. Yu, L. Zaslavsky, J. Zhang, and E. E. Bolton. 2023. "Pubchem 2023 update." *Nucleic Acids Research* 51 (D1): D1373–80. doi:10.1093/nar/gkac956.

Kresse, G., and J. Furthmüller. 1996. "Efficiency of Ab-Initio Total Energy Calculations for Metals and Semiconductors Using a Plane-Wave Basis Set." *Computational Materials Science* 6: 15–50.

Lee, P. L., D. Shu, M. Ramanathan, C. Preissner, J. Wang, M. A. Beno, R. B. Von Dreele, L. Ribaud, C. Kurtz, S. M. Antao, X. Jiao, and B. H. Toby. 2008. "A Twelve-Analyzer Detector System for High-Resolution Powder Diffraction." *Journal of Synchrotron Radiation* 15: 427–32.

Macrae, C. F., I. Sovago, S. J. Cottrell, P. T. A. Galek, P. McCabe, E. Pidcock, M. Platings, G. P. Shields, J. S. Stevens, M. Towler, and P. A. Wood. 2020. "Mercury 4.0: From Visualization to Design and Prediction." *Journal of Applied Crystallography* 53: 226–35.

Materials Design. 2016. *MedeA 2.20.4*. Angel Fire, NM, Materials Design Inc.

MDI. 2023. *JADE Pro Version 8.3*. Livermore, CA, Materials Data.

Peintinger, M. F., D. Vilela Oliveira, and T. Bredow. 2013. "Consistent Gaussian Basis Sets of Triple-Zeta Valence with Polarization quality for Solid-State Calculations." *Journal of Computational Chemistry* 34: 451–9.

Silk Scientific. 2013. *UN-SCAN-IT 7.0*. Orem, UT, Silk Scientific Corporation.

Spackman, P. R., M. J. Turner, J. J. McKinnon, S. K. Wolff, D. J. Grimwood, D. Jayatilaka, and M. A. Spackman. 2021. "Crystalexplorer: A Program for Hirshfeld Surface Analysis, Visualization and Quantitative Analysis of Molecular Crystals." *Journal of Applied Crystallography* 54: 1006–11. doi:10.1107/S1600576721002910.

Stephens, P. W. 1999. "Phenomenological Model of Anisotropic Peak Broadening in Powder Diffraction." *Journal of Applied Crystallography* 32: 281–9.

Sykes, R. A., P. McCabe, F. H. Allen, G. M. Battle, I. J. Bruno, and P. A. Wood. 2011. "New Software for Statistical Analysis of Cambridge Structural Database Data." *Journal of Applied Crystallography* 44: 882–6.

Tanaka, K., and T. Ueto. 2019. "Novel Crystal of Tetracyclic Compound." European Patent EP3135671 B1.

Toby, B. H., and R. B. Von Dreele. 2013. "GSAS II: The Genesis of a Modern Open Source All Purpose Crystallography Software Package." *Journal of Applied Crystallography* 46: 544–9.

Tomar, V. S., A. Azim, N. Gupta, S. Lahiri, and W. Cabri. 2019. "A Process for Preparing Alectinib or a Pharmaceutically Acceptable Salt Thereof." International Patent Application WO2019/008520 A1.

Tomar, V. S., A. Azim, N. Gupta, S. Lahiri, and W. Cabri. 2020. "A Process for Preparing Alectinib or a Pharmaceutically Acceptable Salt Thereof." United States Patent Application US2020/0140427 A1.

van de Streek, J., and M. A. Neumann. 2014. "Validation of Molecular Crystal Structures from Powder Diffraction Data with Dispersion-Corrected Density Functional Theory (DFT-D)." *Acta Crystallographica Section B: Structural Science, Crystal Engineering and Materials* 70: 1020–32.

Wang, J., B. H. Toby, P. L. Lee, L. Ribaud, S. M. Antao, C. Kurtz, M. Ramanathan, R. B. Von Dreele, and M. A. Beno. 2008. "A Dedicated Powder Diffraction Beamline at the Advanced Photon Source: Commissioning and Early Operational Results." *Review of Scientific Instruments* 79: 085105.

Wavefunction, Inc. 2022. *Spartan '20. V. 1.1.4*. Irvine, CA, Wavefunction Inc.